Large-eddy simulations and turbulent combustion model analysis of a dual-mode scramjet combustor

By W. L. Chan† AND M. Ihme

1. Motivation and objectives

Due to their favorable characteristics of reduced payload-cost and high-Mach efficiency, scramjets have been identified as an attractive high-speed propulsion concept (Bertin & Cummings 2003). However, because of stringent operating conditions, accurate and comprehensive physical testings of this type of air-breathing propulsion system have not been feasible, thus preventing the widespread utilization of scramjets. In order to address the lack of reliable test data, numerical simulations provide opportunities to guide the design of scramjet engines. Specifically, the large-eddy simulation (LES) methods have demonstrated promising capabilities to describe key features in supersonic combustion configurations (Fureby 2012; Fulton *et al.* 2014; Saghafian *et al.* 2015).

To advance the development of numerical techniques for the design of scramjet engines, the National Center for Hypersonic Combined-Cycle Propulsion program (McDaniel *et al.* 2009) supported a series of dual-mode scramjet experiments, performed at the University of Virginia's Supersonic Combustion Facility. Non-intrusive diagnostic techniques that have been implemented include focused Schlieren and stereoscopic particle image velocimetry (Rockwell Jr. *et al.* 2014), coherent anti-Stokes Raman spectroscopy (CARS) (Cutler *et al.* 2014), and planar laser-induced fluorescence (Johansen *et al.* 2014), providing measurements of density gradients, velocity fields, hydroxyl radical concentration, temperature, and species mole-fractions.

The objective of the current study is to characterize the University of Virginia's operating point A (UV-A) experiments through a numerical investigation. In this work, a comparative study of two turbulent combustion models, namely the compressible flamelet/progress variable (FPV) model (Pečnik *et al.* 2012) and the laminar finite-rate chemistry (FR) approximation. All simulations are performed with a compressible reacting LES solver, CHRIS (Brès *et al.* 2013), and a detailed hydrogen-air reaction mechanism (Burke *et al.* 2011). To facilitate an objective assessment of the combustion models, all computations are performed with identical grid-quality, subgrid turbulence closure, and time-advancing scheme throughout.

The geometry, boundary and operating conditions, and computational setup are presented in the next section. Then, statistical results from the experiment and both simulations are compared, followed by an analysis of the effects of the combustion model by cross-referencing the two numerical datasets and discussions of the evaluations. The paper finishes with conclusions.

2. Experimental configuration and computational setup

The geometry and boundary conditions of the computational domain are shown in Figure 1(a,b). Note that this domain covers only a portion of the entire UV-A scramjet

† University of Michigan, Ann Arbor MI

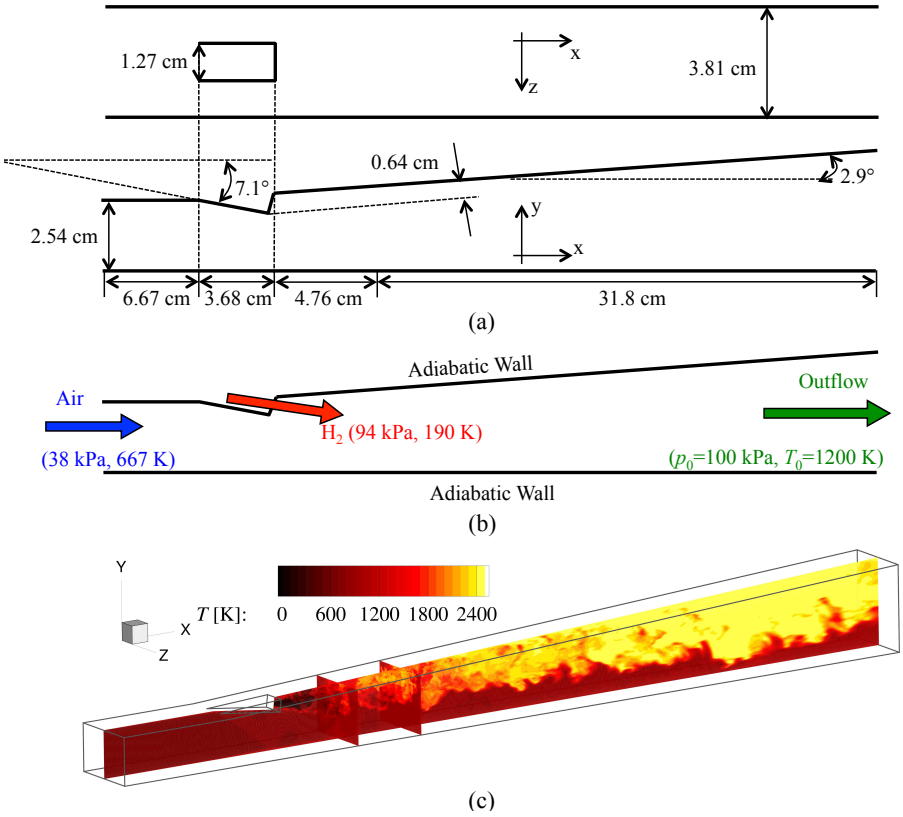

FIGURE 1. Schematic illustration of the geometry (a) and boundary conditions (b) of the UV-A scramjet configuration. As indicated by the various arrows, the general direction of the bulk flow is from left to right. An isometric view of the configuration (c) is provided to show the principal planes-of-interest. The fuel injection port (not shown) has a diameter of $d = 2.54$ mm.

configuration, namely the isolator, combustor, and extender sections. Instead of including the upstream converging-diverging nozzle, a uniform flow of air with Mach 2 static condition is imposed at the inflow plane. The fuel injection is described by a uniform mean flow of pure hydrogen with Mach 1.7 static condition. Artificially generated turbulence is introduced to the mean fuel-flow to represent the turbulent flow dynamics of the fuel jet. The global equivalence-ratio that corresponds to these inflow conditions is 0.17, indicating an overall fuel-lean combustion regime. All walls are prescribed by the no-slip and adiabatic conditions. The outflow plane is assigned by convective-outflow conditions. Figure 1(c) shows the isometric view of the UV-A scramjet combustor, emphasizing the principal planes-of-interest, namely the centerplane ($z = 0$) and two cross-sections ($x = 7.5$ cm and $x = 11.3$ cm), which coincide with two of the four CARS-measurement locations (Cutler *et al.* 2014).

The flow-through time is defined with respect to the length of the computational domain and the fuel injection speed, and is equal to 0.21 ms. Currently, turbulence closures for the filtered momentum and subgrid mixture-fraction variance equations are provided by the Vreman eddy-viscosity subgrid-scale (SGS) model (Vreman 2004) and spectral argument, respectively. In addition, turbulence/chemistry interaction (TCI) is either closed by the compressible FPV combustion model (Pečnik *et al.* 2012), or omitted

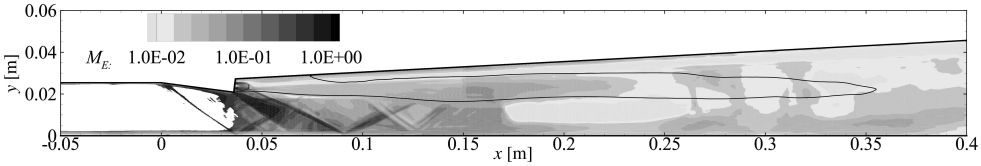

FIGURE 2. Pope's criterion (Pope 2004) along the centerplane. The iso-line denotes the stoichiometric mixture fraction $Z_{\rm st} = 0.0285$.

in the finite-rate FR-closure. The reaction is represented by a detailed hydrogen-air mechanism consisting of nine species and 19 elementary reactions (Burke *et al.* 2011).

The computational domain is discretized by a mixed hexagonal-prism mesh with the ratio of prism to hexagonal elements kept minimal, so that the grid is largely regular. The computational grid comprises of approximately 40 million control-volumes. The adequacy of this level of grid-resolution for LES of the UV-A configuration can be evaluated according to Pope's criterion (Pope 2004)

$$M_E = \frac{\langle \widetilde{k}_t' \rangle}{\langle \widetilde{K}_E \rangle + \langle \widetilde{k}_t' \rangle} \ , \tag{2.1}$$

where $\widetilde{k}_t'$ is the unresolved kinetic energy provided by the SGS model, $\widetilde{K}_E = 0.5(\widetilde{u}_i\widetilde{u}_i - \langle\widetilde{u}_i\rangle\langle\widetilde{u}_i\rangle)$ is the turbulent kinetic energy of the resolved motions, and the angle brackets $\langle\ \rangle$ indicate time-average quantities. The value of M_E is bounded between 0 and 1, corresponding to a direct numerical (all scales resolved) and a Reynolds-averaged Navier-Stokes (all scales modeled) simulation, respectively. Pope suggested that $M_E \leq 0.2$ is an appropriate standard for LES.

Pope's criterion corresponding to the current grid is illustrated in Figure 2, showing that the threshold of $M_E \leq 0.2$ is satisfied for a dominant part of the computational domain. The areas where $M_E > 0.2$ coincide with the vicinities of shocks and expansion waves. Thus, the current grid is sufficient for LES of the UV-A configuration, particularly since regions critical for chemical reactions are all within Pope's M_E-threshold. One caveat in the analysis of Pope's criterion is the singular behavior of M_E in laminar-flow regime, where the denominator in Eq. (2.1) will approach zero. For this reason, regions in Figure 2 where $\langle \widetilde{K}_E \rangle \leq 1$ J/kg have been blanked out so that large M_E that corresponds to flow laminarity is differentiated from that caused by insufficient resolution.

3. Results and discussion

In this section, simulation results will be assessed through various evaluations, beginning with qualitative and quantatitive comparisons with available experimental measurements in terms of mean temperature profile and top-wall pressure distribution, respectively. Then, the physical and conditional results of the two simulations will be compared to further evaluate the significance of turbulent combustion model, followed by a discussion on the findings from these evaluations.

3.1. *Simulation results and measurement comparisons*

The qualitative mean temperature comparisons are shown in Figures 3 and 4 for the cross-sections at $x = 7.5$ cm and $x = 11.3$ cm, respectively. From Figure 3, the FPV-result can be seen to be in slightly better agreement than its FR counterpart in preserving a toroidal flame structure that is hotter on the upper side, but clearly underpredicts the

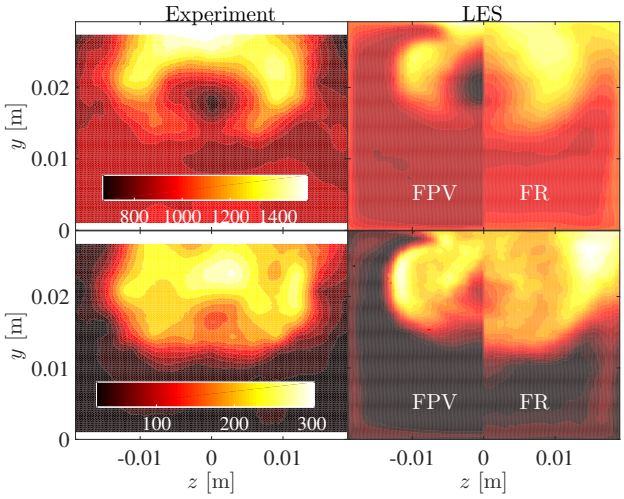

FIGURE 3. Cross-sectional profiles of mean temperature (top) and RMS (bottom) at $x = 7.5$ cm.

reactant-mixing rate. The underprediction in mixing results in a larger fuel core in the FPV-result than the CARS-profile, as shown by comparing the area of low temperature of the two results within the toroid. In contrast, results from te FR-simulations show noticeably overprediction of the reaction-rate, exhibiting a hotter fuel core and thus less-defined flame-ring than the other two results. Both simulations have apparently higher peak RMS values than the experiment, suggesting that the numerical temperature fluctuations are more dominant than the physical fluctuations. The spreading of the RMS profiles indicates that the spatial-range of intermittency of the FR-case is closer to the experimental measurements than that of the FPV-simulation.

A general improvement in the discrepancies with CARS-measurements is observed with increasing streamwise distance, as indicated by comparing the results in Figure 4, to that at $x = 7.5$ cm of Figure 3. For instance, the spanwise spreading of the flame ranges approximately between $z = \pm 1.5$ cm for both experimental and simulation results. Also, the peak fluctuation intensity, which resides within the mixing layer, is approximately 20% of the maximum mean temperature value for all results. While the aforementioned underprediction of the mixing rate in the FPV-result is still discernible in Figure 4, the differences from CARS-measurements are significantly smaller than seen in Figure 3. On the contrary, the overprediction of reaction-rate by the FR-model at $x = 7.5$ cm seemingly has no significant effect on the current downstream plane, where the FR mean temperature exhibits the smallest flame area and lowest value among the three results. The last observation suggests that the omission of TCI in the FR-case may not be as important downstream as it is at the flameholding recirculation region ($3 \lesssim x \lesssim 7$ cm).

The top-wall pressure distribution, which is relevant to the amount of thrust generated from a scramjet, is evaluated in Figure 5. Clearly, the simulations provide reasonably accurate predictions for this measure, showing a generally good agreement with the experiments (symbols). In the region between $5 \leq x \leq 7$ cm, the reacting FPV-result (thin solid line) shows an underprediction of approximately 30%. Conversely, the reacting FR-result (thickened solid line) appears to agree well with the measurement in the same region, but subsequently overpredicts the pressure by approximately 8% at $7 \leq x \leq 15$ cm. This behavior of the FR-result indicates that: (i) the underprediction by the FPV-

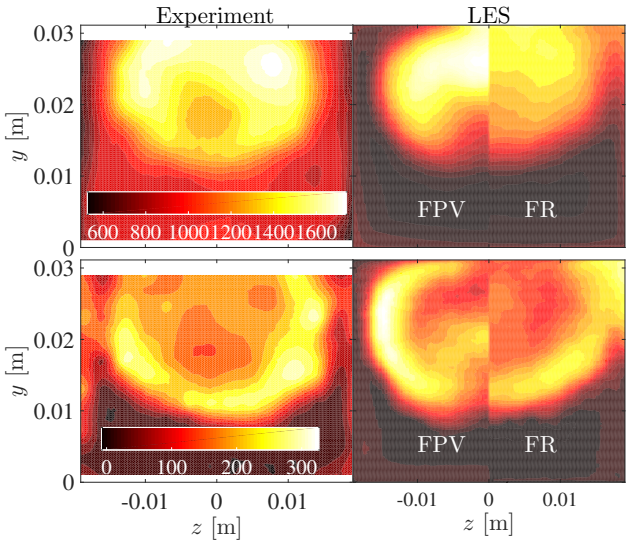

FIGURE 4. Cross-sectional profiles of mean temperature (top) and RMS (bottom) at $x = 11.3$ cm.

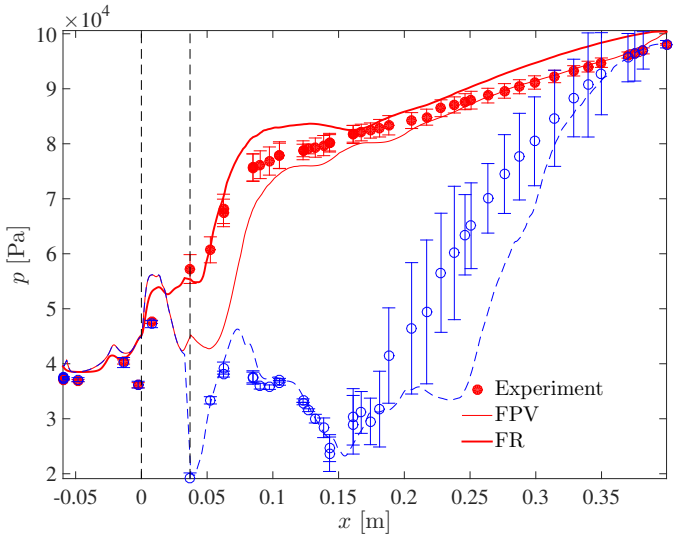

FIGURE 5. Top-wall pressure distribution in the streamwise-direction for the reacting (filled symbol, solid lines) and mixing (open symbol, dashed line) cases. The error bars of the measurements correspond to the 95% confidence-intervals. The two vertical lines, in increasing x, denote the compression ramp leading-edge and fuel-injection port. Only one line is shown for the mixing case since the combustion model is irrelevant.

model is attributed to the aforementioned undermixing and can benefit from an increase in the reaction-rate; and (ii) the reaction-rate in the FR-case is overcompensating, hence is likely to be higher than that in the experiments. Beyond $x \approx 15$ cm, both simulation results agree well with the measurements and each other.

Further insight can be extracted by comparing the non-reacting (open symbol, dashed

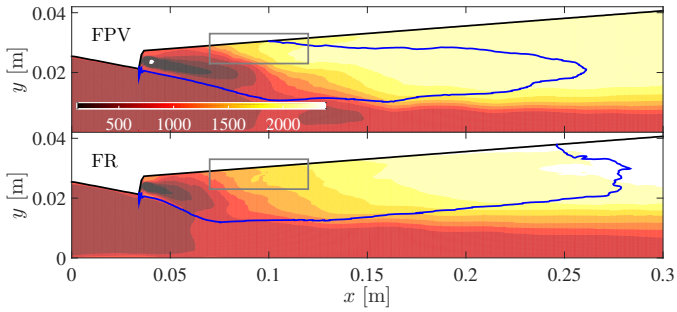

FIGURE 6. Mean temperature profile of the FPV (top) and FR (bottom) cases along the centerplane. The thickened iso-line refers to stoichiometric mixture-fraction $Z_{\mathrm{st}} = 0.0285$, while the box denotes the flame-stabilization region.

line) and reacting (filled symbol, solid lines) solutions. For instance, the non-reacting results between $5 \leq x \leq 15$ cm is in discernibly good agreement with the corresponding non-reacting measurements, suggesting that an inadequate amount of reaction may be the root of the misprediction of the top-wall pressure. This inaccurate description of reaction is possibly a consequence of the misrepresentation of the mixing rate, as suggested by the aforementioned underpredicted mixing rate of the FPV-case. On the other hand, the underprediction for the non-reacting simulation result between $20 \leq x \leq 30$ cm may be attributed to an inadequate grid-resolution. The reacting simulations, however, agree well with the experiments in the stated region because combustion-induced dilatation tends to relax the requirement on the grid-resolution.

3.2. *Turbulent combustion model analyses*

In the following, the sensitivity of the simulation results to the turbulent combustion model will be assessed by considering mean temperature along the centerplane, shown in Figure 6. Consistent with the cross-section analyses, the FR-model predicts a noticeably higher upstream reaction-rate than the FPV-case, as indicated by the shorter fuel-jet penetration and earlier temperature rise. The initial is characterized by the area of low temperature ($T < 500$ K), while the latter is denoted by the mean streamwise location where temperature first exceeds the crossover temperature of 1000 K. This overprediction in the reaction-rate by the FR-model is possibly related to the omission of turbulence-reaction coupling, which will suppress the reaction-rate at the vicinity of fuel injection with intense mixing and high strain on the reactants.

From Figure 6, the FR-result can be seen to increase at a lower rate (i.e. smaller $\partial T/\partial x$) than its FPV counterpart, despite exceeding crossover temperature earlier than the FPV temperature. This slower rise in temperature is also reflected in Figure 4, where the temperature in the FR-result is lower than both measurements and FPV solutions, and is attributed to the localization of the overprediction in reaction-rate by the FR-model at the flameholding recirculation region (window nearer to the fuel injection point in Figure 6). The downstream insensitivity to these upstream discrepancies, introduced in the top-wall pressure comparison (cf. Figure 5), is discernable in the current results as well, where the two simulations are qualitatively similar beyond $x = 15$ cm. This loss of upstream conditions is consistent with the aforementioned general improvement with increasing streamwise distance in both results.

To deepen the understanding of the UV-A scramjet combustor, the statistical conditional results of the configuration are evaluated at several critical locations in terms of the

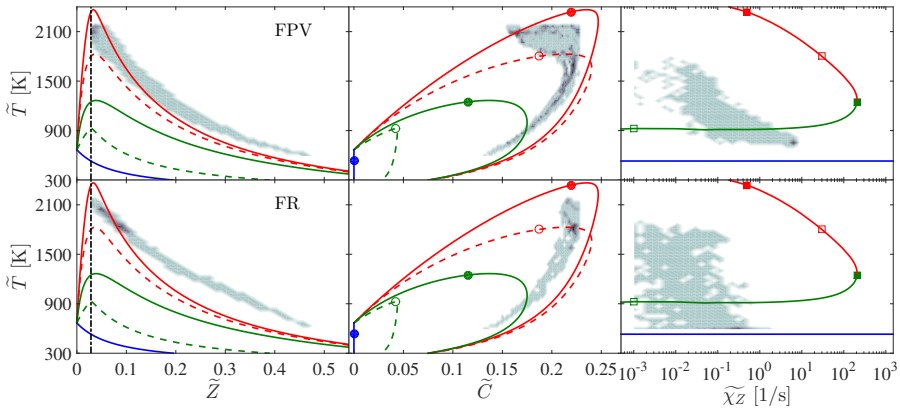

FIGURE 7. Joint PDF's of temperature with mixture-fraction (left), progress-variable (center), and scalar-dissipation rate (right) in the flame-stabilization region of the FPV (top) and FR (bottom) simulations. The solid and dashed lines correspond to the filled and open squares on the right figure, respectively, while the vertical black line and circles denote the stoichiometric mixture-fraction $Z_{\mathrm{st}} = 0.0285$.

joint probability-density-functions (PDF) of temperature, $\widetilde{T}$, with three other variables, namely mixture-fraction ($\widetilde{Z}$), progress-variable ($\widetilde{C}$), and scalar-dissipation rate ($\widetilde{\chi_Z}$). The results that correspond to the configuration's flame-stabilization zone is shown in Figure 7; this zone is defined by the spatial range where the mean temperature in both simulations exceed the crossover temperature of 1000 K and is indicated by the window in Figure 6. Various laminar flamelet solutions, indicated by the lines and symbols, are also provided in Figure 7 to extract any intrinsic flamelet properties of the joint-PDF's.

Considering the statistical results in Figure 7, in particular the $\widetilde{T}$-$\widetilde{Z}$ and $\widetilde{T}$-$\widetilde{C}$ distributions, the FPV-results are in a discernibly good agreement with flamelet solutions of the stable upper branch of the S-shaped curve shown in the right panels. Note that the laminar flamelet solutions were calculated at a constant pressure of 1 bar, while the FPV-results accounted for pressure-variation effects, so the slightly higher FPV temperature than the maximum flamelet temperature seen at the fuel-rich side of the $\widetilde{T}$-$\widetilde{Z}$ plot is plausible. In contrast, the $\widetilde{T}$-$\widetilde{Z}$ plot of the FR-case only agrees with stable-upper flamelet solutions around stoichiometric composition and exceeds the maximum flamelet temperature profile for $\widetilde{Z} > 0.1$. This increased fuel-rich temperature is possibly related to the aforementioned overprediction of the reaction-rate by the FR-simulations (cf. Figure 6), which in turn seems to advocate a lower dissipation rate than the FPV-case by comparing the $\widetilde{T} - \widetilde{\chi_Z}$ plots. In addition, the $\widetilde{T} - \widetilde{\chi_Z}$ distributions suggest that temperature is more correlated to the scalar-dissipation rate in the FPV-case than in the FR-case, as can be deduced from the initial's scattering that is clearly well-fitted by a definite slope. Both results appear to be well-represented by the flamelet solutions in the $\widetilde{T}$-$\widetilde{C}$ plots, implying a general correlation between $\widetilde{T}$ and $\widetilde{C}$ that is indifferent to the combustion model.

3.3. *Discussions*

Through comparisons with measurements, both simulation results are observed to accurately capture essential physical behaviors of the UV-A scramjet, including the dependence of flameholding on recirculation of reaction products, relevance of reactant mixing to reaction-rates, and occurrence of an adverse pressure gradient across the combustor. In light of the simple boundary conditions and model closures of the simulations, such simu-

lation performance is encouraging, indicating the applicability and potential of numerical techniques in describing scramjet phenomena.

Further analyses that focus on the turbulent combustion models showed that: (i) the omission of TCI will lead to an overprediction of the reaction-rate that tends to localize near the fuel injection port; and (ii) the combustion models behave similarly, exhibiting a general agreement with the flamelet formulation. Considering the differences in the fundamental assumptions of the two combustion models, which are reflected by the physical discrepancies between the two results shown in Figures 3–4 and 6, the similar flamelet-behavior of the two models is noteworthy, suggesting that the flamelet concept is inherently applicable to the UV-A scramjet combustor. Therefore, the application of flamelet-type turbulent combustion models in the current configuration appears valid. However, such application may require the consideration of flamelet unsteadiness so that transient events such as flame-ignition and flame-quenching can be captured accurately.

From a cost perspective, the inherent flamelet applicability of the UV-A scramjet combustor renders the FPV-model a better closure than the FR-approximation, for the reason that the initial is more efficient (approximately three times in the current work) due to its smaller equation set that significantly reduces system stiffness. Additionally, the FPV-model accounts for TCI through the method of presumed PDF (Peters 2000).

Based on the current findings, the UV-A configuration is clearly a useful setup for the continued development of flamelet-based combustion models in supersonic reacting regimes. In this regard, aspects of flamelet models that can be extended include the introduction of higher-order flamelet effects (Ihme & See 2010; Scholtissek *et al.* 2015) and more accurate description of PDF distributions (Koo *et al.* 2011; Coclite *et al.* 2015). With regards to improving the simulation predictions, hybrid combustion models of both classes of reaction-transport (e.g. FPV, flame-prologation in intrinsic low-dimensional manifolds (Gicquel *et al.* 2000)) and chemistry (i.e. detailed/skeletal reaction kinetics) manifolds can be systematically constructed and optimized using the concept of Pareto-efficiency developed by Wu *et al.* (2015).

4. Conclusions

A numerical study that aims to deepen the understanding of the characteristics of a dual-mode scramjet combustor was conducted. The geometry of the scramjet of interest corresponds to the configuration A of the University of Virginia's dual-mode scramjet experiments, which is designed to emulate Mach 5 flight conditions. The simulations were performed in the context of large-eddy simulations, using a compressible reacting LES solver and a detailed hydrogen/air mechanism. All relevant numerics are kept identical, except for the turbulent combustion model, where the flamelet/progress-variable formulation and laminar finite-rate approximation were separately considered.

Through comparison with measurements, both combustion closures were found to perform comparably, generally capturing the essential physical behaviors of the experiments with reasonable accuracies. The two simulation results were further examined through model analyses that consist of the comparison of simulation results and characterization of the configuration's intrinsic flame behaviors. The first study essentially showed that the omission of turbulence-reaction coupling will affect the simulation's accuracy by overpredicting the reaction-rate, but this misrepresentation is apparently localized at the upstream fuel injection vicinity, and will eventually be lost as the flow traverse downstream. As a result, a general improvement in both simulations with streamwise distance

was observed. With regards to the flame regime characterization, joint probability density functions of various flow and thermochemical variables were extracted, showing that the flamelet formulation is applicable regardless of the turbulent combustion model. This indifference to the closure model suggests that the flamelet-behavior may be an inherent character of the current configuration. The applicability of flamelet-based combustion models in the supersonic reacting regime is therefore demonstrated.

Acknowledgments

Financial support through AFOSR under Award No. FA9550-11-1-0031 is gratefully acknowledged.

REFERENCES

Bertin, J. J. & Cummings, R. M. 2003 Fifty years of hypersonics: where we've been, where we're going. *Prog. Aerospace Sci.* **39**, 511–536.

Brès, G. A., Ham, F. E., Nichols, J. W. & Lele, S. K. 2013 Nozzle wall modeling in unstructured large eddy simulations for hot supersonic jet predictions. *AIAA Paper* 2013-2142.

Burke, M. P., Chaos, M., Ju, Y., Dryer, F. L. & Klippenstein, S. J. 2011 Comprehensive H2/O2 kinetic model for high-pressure combustion. *Int. J. Chem. Kinet.* **44** (7), 444–464.

Coclite, A., Pascazio, G., De Palma, P., Cutrone, L. & Ihme, M. 2015 An SMLD joint PDF model for turbulent non-premixed combustion using the flamelet progress-variable approach. *Flow, Turb. Combust.* **95**, 97–119.

Cutler, A. D., Magnotti, G., Cantu, L., Gallo, E., Rockwell, R. & Goyne, C. 2014 Dual-pump coherent anti-Stokes Raman spectroscopy measurements in the dual-mode scramjet. *J. Prop. Power* **30** (3), 539–549.

Fulton, J. A., Edwards, J. R., Hassan, A. H., McDaniel, J. C., Goyne, C. P., Rockwell, R. D., Cutler, A. D., Johansen, C. T. & Danehy, P. M. 2014 Large-eddy/Reynolds-averaged Navier-Stokes simulations of reactive flow in dual-mode scramjet combustor. *J. Prop. Power* **30** (3), 558–575.

Fureby, C. 2012 LES for supersonic combustion. *AIAA Paper* 2012-5979.

Gicquel, O., Darabiha, N. & Thévenin, D. 2000 Laminar premixed hydrogen/air counterflow flame simulations using flame prolongation of ildm with differential diffusion. *Proc. Combust. Inst.* **28**, 1901–1908.

Ihme, M. & See, Y. C. 2010 Prediction of autoignition in a lifted methane/air flame using an unsteady flamelet/progress variable model. *Combust. Flame* **157**, 1850–1862.

Johansen, C. T., McRae, C. D., Danehy, P. M., Gallo, E. C. A., Cantu, L. M. L., Magnotti, G., Cutler, A. D., Rockwell Jr., R. D., Goyne, C. P. & McDaniel, J. C. 2014 OH PLIF visualization of the UVa supersonic combustion experiment: configuration A. *J. Vis.* **17**, 131–141.

Koo, H., Donde, P. & Raman, V. 2011 A quadrature-based LES/transported probability density function approach for modeling supersonic combustion. *Proc. Combust. Inst.* **33**, 2203–2210.

McDaniel, J. C., Chelliah, H., Goyne, C. P., Edwards, J. R., Givi, P. &

Cutler, A. D. 2009 Us National Center for Hypesonic Combined Cycle Propulsion: An overview. *AIAA Paper* 2009-7280.

Peters, N. 2000 *Turbulent Combustion*. Cambridge University Press.

Pečnik, R., Terrapon, V. E., Ham, F., Iaccarino, G. & Pitsch, H. 2012 Reynolds-averaged Navier-Stokes simulations of the HyShot II scramjet. *AIAA J.* **50**, 1717–1732.

Pope, S. B. 2004 Ten questions concerning the large-eddy simulation of turbulent flows. *New J. Phys.* **6** (35), 1–24.

Rockwell Jr., R. D., Goyne, C. P., Rice, B. E., Kouchi, T., McDaniel, J. C. & Edwards, J. R. 2014 Collaborative experimental and computational study of a dual-mode scramjet combustor. *J. Prop. Power* **30** (3), 530–538.

Saghafian, A., Shunn, L., Philips, D. A. & Ham, F. 2015 Large eddy simulations of the HIFiRE scramjet using a compressible flamelet/progress variable approach. *Proc. Combust. Inst.* **35**, 2163–2172.

Scholtissek, A., Chan, W. L., Xu, H., Hunger, F., Kolla, H., Chen, J. H., Ihme, M. & Hasse, C. 2015 A multi-scale asymptotic scaling and regime analysis of flamelet equations including tangential diffusion effects for laminar and turbulent flames. *Combust. Flame* **162**, 1507–1529.

Vreman, A. W. 2004 An eddy-viscosity subgrid-scale model for turbulent shear flow: Algebraic theory and applications. *Phys. Fluids* **16** (10), 3670–3681.

Wu, H., See, Y. C., Wang, Q. & Ihme, M. 2015 A Pareto-efficient combustion framework with submodel assignment for predicting complex flame configurations. *Combust. Flame* **162**, 4208–4230.